ACS OMEGA

http://pubs.acs.org/journal/acsodf

Article

Spontaneous Transport Mechanics of Water Droplets under a Synergistic Action of Designed Pattern and Non-Wetting Gradient

Weilan Liu, Yang Lu, Yizhou Shen,* Haifeng Chen, Yaru Ni,* and Yangjiangshan Xu

Cite This: *ACS Omega* 2023, 8, 16450−16458

Read Online

ACCESS | Metrics & More | Article Recommendations | Supporting Information

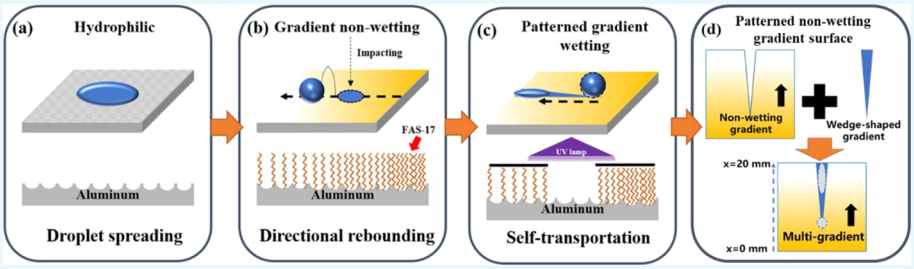

ABSTRACT: The controllable spontaneous transport of water droplets on solid surfaces has a broad application background in daily life. Herein, a patterned surface with two different non-wetting characteristics was developed to control the droplet transport behavior. Consequently, the patterned surface exhibited great water-repellant properties in the superhydrophobic region, and the water contact angle reached 160° ± 0.2°. Meanwhile, the water contact angle on the wedge-shaped hydrophilic region dropped to 22° after UV irradiation treatment. On this basis, the maximum transport distance of water droplets could be observed on the sample surface with a small wedge angle of 5° (10.62 mm), and the maximum average transport velocity of droplets was obtained on the sample surface with a large wedge angle of 10° (218.01 mm/s). In terms of spontaneous droplet transport on an inclined surface (4°), both the 8 μL droplet and 50 μL droplet could move upward against gravity, which showed that the sample surface possessed an obvious driving force for droplet transport. Surface non-wetting gradient and the wedge-shaped pattern provided unbalanced surface tension to produce the driving forces in the process of droplet transport, and the Laplace pressure as well is produced inside the water droplet during this process. This work provides a new strategy to develop a patterned superhydrophobic surface for droplet transport.

INTRODUCTION

Controllable spontaneous water droplet transport has important significance in multiple fields, such as microfluidic devices,[1−3] water harvesting,[4−6] and water−oil separation.[7−9] Surfaces with controlled wetting properties are widely acceptable materials to achieve self-transport of droplets.[10,11] In recent years, researchers have modified various surfaces with non-wetting gradient to realize the facility of unidirectional water self-transport.[12,13] For instance, Chaudhury and Whitesides[14] experimentally achieved droplet transport on a wetting gradient surface, and a 1 μL droplet moved upward on an inclined surface with a transport velocity of 1−2 mm/s. There are some related literature reporting the steering of droplets using various surfaces. For instance, Leng et al.[15] summarize the mechanisms of water droplet manipulation on various biological surfaces. Yang et al.[16] explored multi-bioinspired SLIPS-patterned surfaces that allow for directional droplet sliding, and precise steering of droplet friction was created by coordinating the heterogeneous wettability of the back of the desert beetle, directional-dependent architecture of the butterfly wing, and ultraslippery configuration of *N. alata*. Yang et al.[17] reported three-dimensional (3D) topological SLIPS with an anisotropic-slippery-Wenzel state; fabricated rice leaflike grooved nanotextured SLIPS can properly shape the droplet footprint to achieve a sliding resistance anisotropy of 109.8 μN.

In recent years, it has been proved that wettability pattern design is the key to achieve spontaneous directional transport, and the wedge-shaped pattern is quite effective and simple to prepare.[18−22] Khoo and Tseng[23] prepared a chemically patterned nanotextured surface with wedge-shaped non-wettability gradient on the aluminum substrate, wherein both microliter and nanoliter droplets could be transported rapidly along the expected direction. Besides, Zheng et al.[24] formulated a wedge-shaped superhydrophobic copper surface with a poly-(dimethylsiloxane) (PDMS) oil layer and systematically discussed the droplet movement on the surface. It is

Received: March 7, 2023
Accepted: April 18, 2023
Published: April 28, 2023

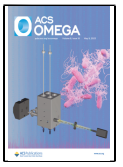

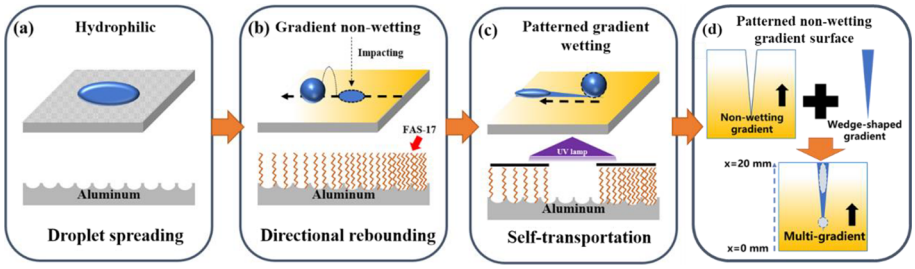

Figure 1. Schematic illustration of the fabrication process of patterned non-wetting gradient surface. (a) Hydrophilic substrate with a micro-nano structure before chemical modification. (b) Gradient non-wetting substrate after FAS-17 modification. (c) Patterned gradient non-wetting substrate after partly exposed in UV irradiation. (d) General schematic of patterned non-wetting gradient surface.

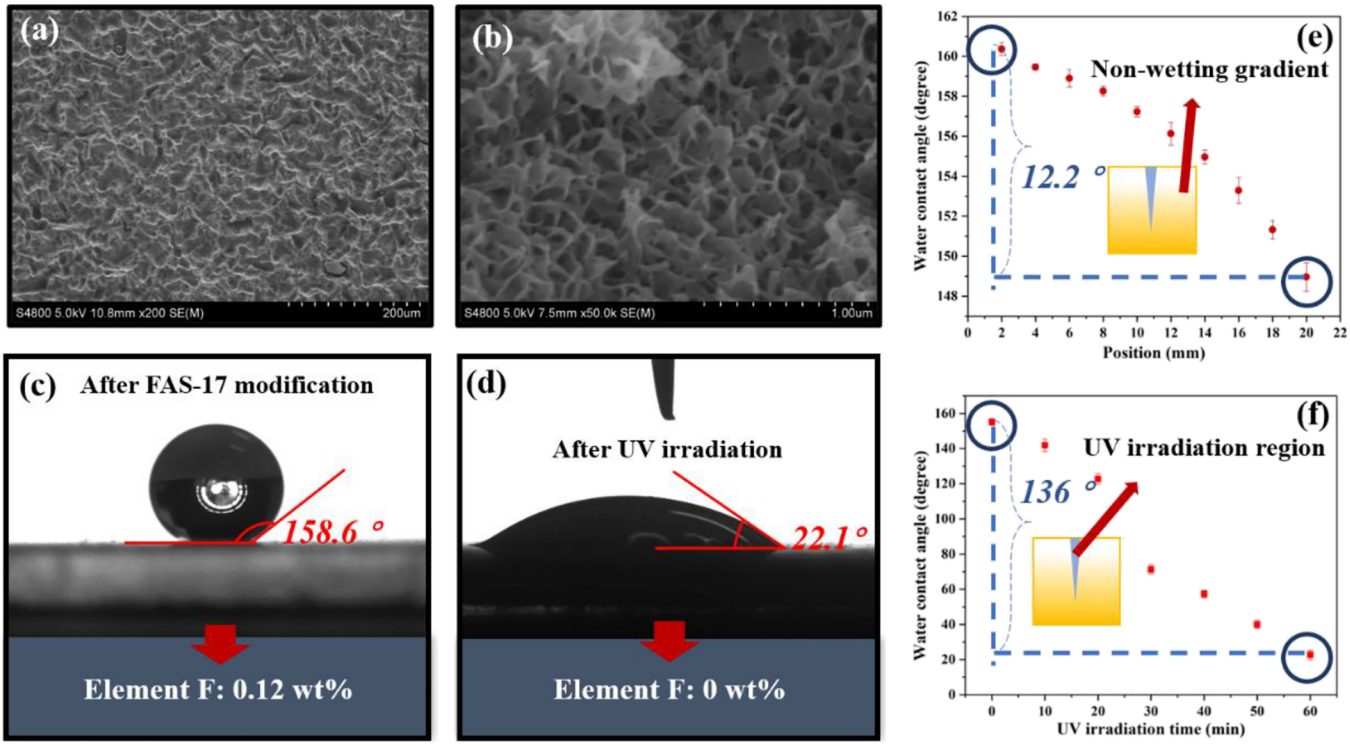

Figure 2. Wettability characteristics of the sample surface. (a) Micro-scale structure of surface (×200). (b) Nano-scale structure of surface (×50,000). (c) Non-wetting sample surface after FAS-17 modification. (d) Hydrophilic sample surface after UV irradiation. (e) Variation of the water contact angle with UV irradiation time from 0 to 60 min.

concluded that non-wettability gradient and wedge-shaped gradient are both beneficial for self-transport of water droplets.[25−29] However, only a few research studies combine these two methods to synergistically achieve spontaneous directional transport of water droplets, and how to effectively enhance the transport velocity and distance of droplet is still an unclear problem.

Herein, gradient non-wetting surfaces were prepared on an aluminum substrate, and the hydrophilic regions were obtained on the substrate by proper ultraviolet irradiation treatment. The surfaces were characterized based on several aspects and the motion behaviors of water droplets were recorded using a high-speed camera. On this basis, some parameters such as the angle of wedge shape, droplet size, and surface inclination angle were adjusted, and the motion characteristics of droplets were analyzed. Finally, the motion law of droplets and the state of driving force during droplet motion were summarized and revealed. The velocity and distance of droplet movement on the surfaces were enhanced to ingratiate diverse applications.

EXPERIMENTAL SECTION

Materials. Deionized water droplets used in this work were obtained from a Milli-Q system. Pure aluminum substrates (99.9%) with a size of 20 mm × 20 mm × 1 mm were obtained from the Beijing Nonferrous Metal Research Institute (Beijing, China). Fluoroalkylsilane (FAS-17) as a modifying agent was purchased from Tokyo Chemical Industry Co. Ltd., Japan. All the chemicals used in this experiment, such as sodium chloride (NaOH) and ethanol, were analytical grade and provided by Sinopharm Chemical Reagent Co. Ltd., China.

Preparation of the Patterned Non-wetting Gradient Surface. The patterned non-wetting gradient surfaces were prepared *via* a facile and inexpensive method. After sample pretreatment, pretreated samples (20 mm × 20 mm × 1 mm) were immersed in 0.05 mol/L sodium chloride solution at 80 °C for 5 min and placed in deionized water at 100 °C for 40 min to grow the nanosheet structures, as shown in Figure 1a. Thereafter, 1 wt % FAS-17 ethanol solution was blended in a small beaker, and the as-obtained samples were vertically hung

https://doi.org/10.1021/acsomega.3c01536
ACS Omega 2023, 8, 16450−16458

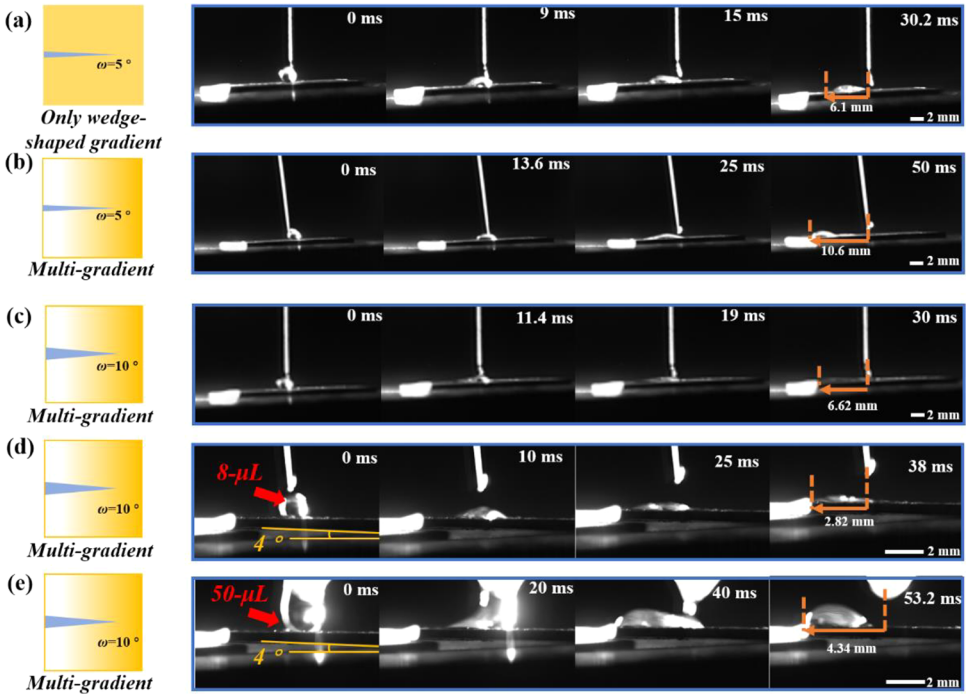

Figure 3. Spontaneous droplet transportation in different situations. (a) On a surface with only a wedge-shaped pattern (ω = 5°). (b) On a surface with both non-wetting gradient and wedge-shaped pattern (ω = 5°). (c) On a surface with both non-wetting gradient and wedge-shaped pattern (ω = 10°). (d) Transportation of an 8 μL droplet on an inclined surface (ω = 10°). (e) Transportation of a 50 μL droplet on an inclined surface (ω = 10°).

above the solution. The samples and beaker were placed in an 80 °C oven for 1 h for gradient modification, and the samples were dried in a 120 °C oven for 2 h to obtain a gradient non-wetting functional surface, as shown in Figure 1b. Finally, hydrophilic patterns were formed on the gradient non-wetting sample surface by selectively exposing the substrates to UV irradiation (300 W, 365 nm) for 1 h using an opaque mask, as shown in Figure 1c. The general schematic diagram is shown in Figure 1d.

Characterizations. A field emission scanning electron microscope (FE-SEM; Hitachi S4800, Japan) was used to observe the morphology of the sample surface at different scales. Surface chemical composition was characterized by EDS after both gradient modification and UV irradiation. Besides, the water contact angle (CA) was measured using a contact angle analyzer (Kruss DSA100, Germany). The water CA on hydrophobic and hydrophilic regions are the average values measured with 8 μL reference water droplets.

Droplet Transport Ability Test. The dynamic transport processes of water droplets (8 μL) on both horizontal surfaces and inclined surfaces were recorded using a 5000-fps firmed high-speed camera (Phantom Mini 100, USA). The transport processes of 50 μL droplets were recorded on the inclined surfaces for comparison. A 0.03 mm-diameter ultrafine syringe needle and a dropper which were modified with FAS-17 for hydrophobicity were selected to obtain microdroplets during tests,

RESULTS AND DISCUSSION

Surface Morphology and Gradient Non-wettability. After sandblasting and chemical etching treatment, uniform micropit structures appear on the sample surfaces, and well-arranged nanosheet structures with a diameter of 100 nm evenly cover the sample surfaces, as shown in Figure 2a,b. Figure 2c,d presents the wetting state after surface chemical modification, wherein the droplet volume is exactly 6 μL. After superhydrophobic modification, the CA of the surface is about 158° due to the rough structures and low surface energy, as shown in Figure 2c,[30,31] which proves that element F is grafted on the sample surfaces (from FAS-17). In comparison, a significant decrease of wettability occurs on the surface after UV irradiation for 1 h. Figure 2d shows that the droplet could spread on the sample surface, and the WCA drops to about 22°. Ultraviolet light has strong oxidizing ability and could oxidize fluoroalkyl at the end of fluorosilane molecules on the surface. Fluoroalkyl gradually changes into hydrophilic hydroxyl with the increase of oxidation time, which greatly increases the surface hydrophilicity.[32−34] Surface composition changes could be found in Figures S1 and S2 in the Supporting Information. After 1 h of UV irradiation, the content of element F could not be detected in the modified areas. The relationship between UV irradiation time and WCA is presented in Figure 2e. The surface hydrophobicity gradually decreases as the irradiation time increase from 0 min to 1 h. In this process, the WCA of the treated regions drops from 158.5° ± 0.2° to 22° ± 0.1° and the huge difference between the superhydrophobic and hydrophilic regions form the unbalanced surface tension, which is advantageous for liquid transport.[33]

Spontaneous Transport Features of Droplets. The complete controlled transport processes of 8 μL droplets on different surfaces are shown in Figure 3a−d, and controlled transport processes of 50 μL droplets are shown in Figure 3e; details could be found in Supporting Videos (S1−S5). In general, the transport distance and transport velocity are two vital factors to evaluate the droplet transport process. Figure 3a−c displays the images of droplet transport on different horizontal patterned surfaces. Water droplets move along the

https://doi.org/10.1021/acsomega.3c01536
ACS Omega 2023, 8, 16450−16458

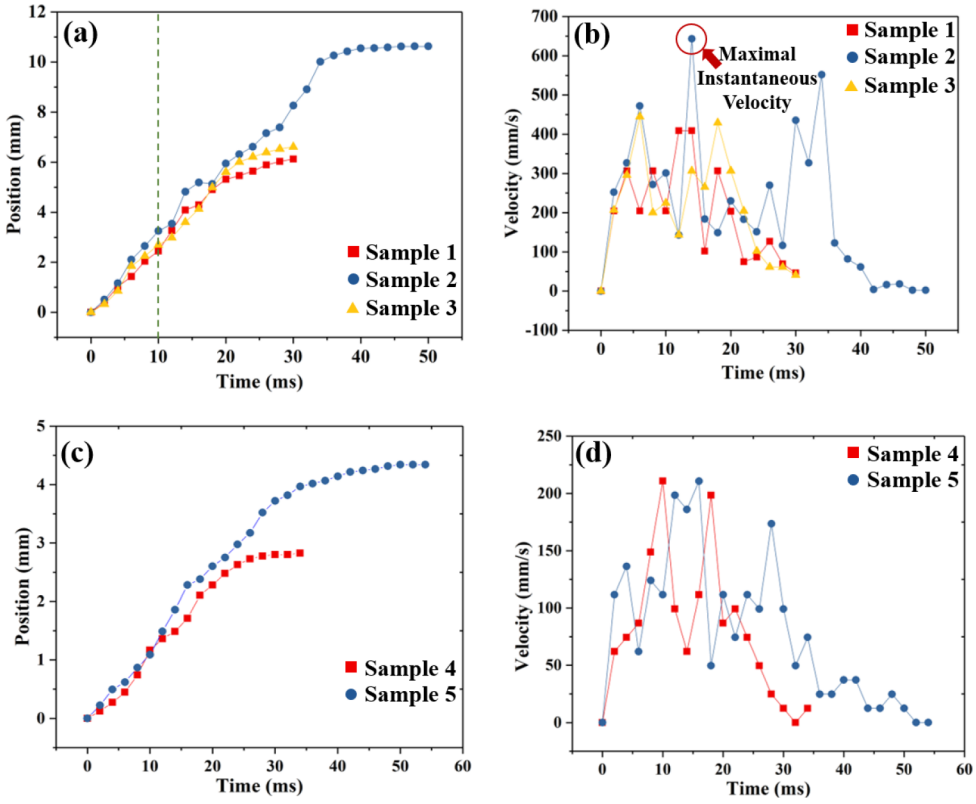

Figure 4. Position and velocity of droplets with different volume. (a) Relation between droplet transport distance and time on different horizontal surfaces. (b) Relation between droplet transport velocity and time on different horizontal surfaces. (c) Relation between transport distance and time of droplets with different volume on inclined surfaces (β = 4°). (d) Relation between transport velocity and time of droplets with different volume on inclined surfaces (β = 4°).

anticipated direction quickly without any external force on the surface with 5° wedge-shaped patterns, as shown in Figure 3a. As a result, water droplets could only be transported for a relatively short distance of 6.1 mm. However, on the surface in Figure 3b, the superhydrophobic regions also have surface chemical gradient apart from the wedge-shaped pattern. When the droplet is released from the tip end of the wedge-shaped pattern, it moves spontaneously toward hydrophilic regions from the superhydrophobic regions. In the above process, a part of the droplet bottom contacts the boundary between the hydrophilic and superhydrophobic regions on the patterned surface, and an unbalanced capillary force drives the droplet motion. Meanwhile, as the droplet diameter is larger than the width of the pattern tip, a part of the droplet bottom contacts the gradient wetting areas on the sample surface and is also subjected to the additional lateral wetting gradient force in the direction of droplet movement. The moving behavior of the water droplet is more prominent on a patterned non-wetting gradient surface than on a sample surface with only the wedge-shaped patterns because of the additional driving force from non-wetting gradient. Furthermore, under the additional driving force, the maximum value of the front section of the droplet deviating from the original position is 10.62 mm, which is a significant improvement in transport distance than that on the sample surface with only wedge-shaped patterns.

The wedge angle ω is an important factor affecting the process of droplet transportation.[35] Thus, wetting patterns with different ω (ω = 5° and ω = 10°) are designed to investigate the role of ω on the droplet transport process. A larger ω means the increase in area of the hydrophilic region, leading to the faster spread velocity of droplet in the transport process, which shortens the transport distance of the water droplet due to the resistance from the hydrophilic region. The results in Figure 3c reveal that the value of maximum transporting displacement on the surface with ω of 10° is 6.62 mm, which is only 62.3% of that value on the surface with ω of 5°.

The transport behavior of different sized droplets on an inclined surface is demonstrated in Figure 3d,e. It is significant to evaluate the sample surface performance to resist gravity. The inclination angle β is fixed at 4°, and the volume of the small droplet and large droplet equaled 8 and 50 μL, respectively. Besides, the wedge angle is selected to be exactly 10° for this experiment. The 8 μL droplet climbs up for a maximum displacement of 2.82 mm in 38 ms, and a 50 μL droplet moves up to 4.34 mm within 53.4 mm, as shown in Figure 3d,e. These results prove that for a certain wedge angle, the larger droplet may move a larger distance.[32]

Droplet Transport Behavior. Transport distance and velocity of droplets on the surfaces are recorded and shown in Figure 4a–d, in order to understand the characteristics of droplet transport, and some notable values in the process (V_{max}, V_{ave}, and V_{10ms}) are also listed in Table 1. Herein, the transport distance and velocity of the front end of the droplet are measured during the whole process. It is noted that both transport distance and velocity of the droplets on the patterned non-wetting gradient surface (Sample 2, Sample 3) are larger than those on the sample without non-wetting gradient (Sample 1), which suggests that the non-wetting gradient provides additional driving force and could be superimposed

https://doi.org/10.1021/acsomega.3c01536
ACS Omega 2023, 8, 16450−16458

Table 1. Droplet Transporting Velocities and Displacements on Different Samples

	wetting gradient	wedge angle (°)	S_{max} (mm)	V_{max} (mm/s)	V_{ave} (mm/s)	V_{10ms} (mm/s)
Sample 1	no	5	6.1	408.7	204	204.38
Sample 2	yes	5	10.62	682.6	212.58	254.61
Sample 3	yes	10	6.61	429.2	218.01	224.82

on the unbalanced capillary force caused by the wedge-shaped pattern in the expected transport direction. Furthermore, the droplets on the surface with a smaller wedge angle (ω = 5°) has a clear advantage in transport distance, and the maximum instantaneous velocity V_{max} reached a high value of 682.6 mm/s, which is larger than those in several aforementioned studies.[23,24,36] However, V_{max} could not fully represent the transport velocity of the droplets. As listed in Table 1, the average velocities on the surface with a larger wedge angle of 10° (218.01 mm/s) are faster than that on the surface with a smaller wedge angle of 5° (212.58 mm/s), which signifies that a larger ω may be beneficial for an overall faster droplet transport behavior.

As the results shown in Figure 4b, the transport velocities of droplets exhibit oscillating characteristics during the whole transport process, which indicates the occurrence of multiple acceleration and deceleration circles. At the initial time, a large driving force is produced when the droplet contacts with both the wedge-shaped pattern region and wetting gradient region, and the front part of the droplet rapidly moves under two combined driving forces. Meanwhile, a major part of the droplet moves forward with a slower velocity under the pull of the front part of the droplet, due to the uneven force inside the droplet. When the front part of the droplet moves forward, the combined driving force gradually decreases due to the lack of pressure difference and reduction of the wetting gradient force, resulting in a significant velocity decrease of the droplet. Subsequently, the major part of liquid flows into the front part through a meniscus during the coalescence of the droplet.[37−40] After the coalescence of the droplet, the volume of the droplet increases, and the thrust produced during the coalescence of the droplet enhances the advancing CA, causing enough driving force for a second acceleration and farther droplet transport. The combined driving force gradually decreases with the motion of the droplet and gradually drops to zero after 2 or 3 acceleration-deceleration processes, resulting in the ending of the transport process. It is noted that the time interval between oscillations is related to ω, as shown in Figure 4b, and the time interval between oscillations is inversely proportional to ω. The time interval between oscillations depends on the flowing velocity of the droplet, and a larger ω cause a wider meniscus, which accelerates the flowing velocity of the liquid inside the droplet.[41] Though the V_{max} (682.6 mm/s) occurs on the surface with a smaller wedge angle, the driving force at the initial position is closely related to the front contact line length between the droplet and wedge-shaped pattern, which means that surfaces with larger ω could create stronger driving forces from the wedge-shaped pattern.[42] However, there is another driving force, non-wetting gradient force, which exists on the patterned sample surface, and the continuous driving force from the non-wetting gradient in initial transport aids to accelerate the movement of the water droplet. For water droplets with the same diameter, the contact area between droplets and superhydrophobic regions is larger on the surface with smaller ω, causing the larger additional driving force from non-wetting gradient. Consequently, under the superposition of the two driving forces, the droplet on the surface with ω of 5° obtains a higher initial velocity. In general, the larger the wedge angle, the stronger the driving force obtained from the wedge pattern, but this does not mean that the droplet has a strong self-transport capacity. Factors such as the driving force provided by the wetting gradient surface and the droplet wetting contact area also influence the droplet self-transport behavior.

It has been proven that droplets have great motion ability on a horizontal surface with both non-wetting gradient and a wedge-shaped pattern; here, the droplet transport behavior is further analyzed on inclined surfaces (Sample 4, Sample 5). Compared with the droplet transport on the horizontal surface, additional resistance force during the transport process increases significantly due to the presence of gravity component mgsinβ. Therefore, as demonstrated in Figure 4c,d, the motion ability of droplets is partially weakened on the inclined surface. For a droplet with a fixed volume, not only transport distance decreases but also the transport velocity is also reduced. For an 8 μL droplet on the inclined surface, the maximum instantaneous velocity V_{max} only reaches a value of 210.8 mm/s, which is only about 50% of that on the horizontal surface.

The transport characteristics of droplets on the inclined surface are similar to those on the horizontal surface, and different sized droplets both underwent multiple acceleration and deceleration circles. It is surprising that larger droplets could move to higher positions with a larger average transport velocity (V_{ave}). Although the 50 μL droplet needs to encounter higher resistance force due to larger mass, it has a larger combined driving force for transport. On the one hand, a larger droplet volume leads to higher advancing CA, providing larger driving force for droplet acceleration. On the other hand, a larger droplet has more contact areas with hydrophobic non-wetting gradient regions, resulting in a larger non-wetting gradient force during transportation. Besides, transport velocity is also related to the degree of wetting difference in superhydrophobic areas and wedge-shaped pattern areas, and the increase of droplet volume means the larger length of contact line between the droplet and wedge-shaped pattern.[43] In fact, the driving forces from non-wetting gradient and the wedge-shaped pattern are both important for the transport of the droplets. The droplet is difficult to achieve self-transport if there is insufficient driving force from non-wetting gradient. The relevant analysis is described in detail in the following section.

Mechanical Analysis of Droplet Transport. In general, droplet movement is suffered from various resistances, such as viscous force ($F_{viscous}$), hysteresis force ($F_{hsyteresis}$), friction force ($F_{friction}$), and surface tension force ($F_{surface\ tension}$). When these resistances are greater than the driving forces, droplets could not achieve self-transport. Before discussing the droplet transport behavior on a patterned non-wetting gradient surface, a simpler situation is considered first. If a water droplet is placed on a homogeneous surface, it is subjected to balanced surface tension (F_s). Figure 5a shows the three-phase contact line of a water droplet placed on a homogeneous surface, and the surface tension force component in the x-axis direction along the contact line could be expressed as:[24]

$$dF_s = \gamma\cos\theta\cos\alpha ds = \gamma R\cos\theta\cos\alpha d\alpha \quad (1)$$

https://doi.org/10.1021/acsomega.3c01536
ACS Omega 2023, 8, 16450−16458

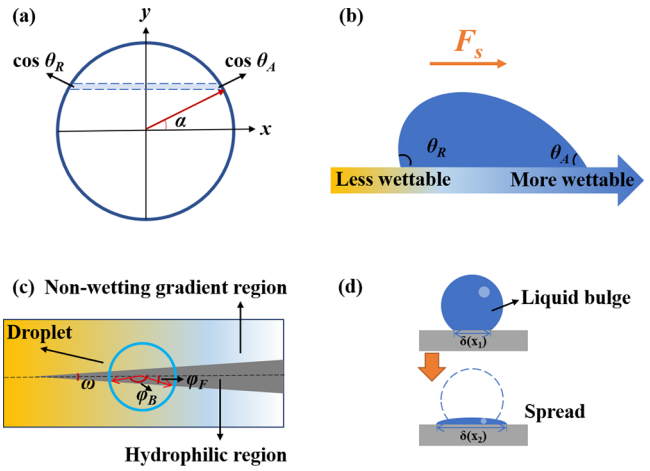

Figure 5. Schematic diagram of driving forces acting on droplets during spontaneous transportation. (a) Three-phase contact line of a droplet on a homogeneous surface. (b) Driving force F_s from wettability gradient. (c) Diagram of three-phase contact line of a droplet on patterned non-wetting gradient surface. (d) Front view of liquid bulge phenomenon.

where γ is surface tension, θ is the CA at the position of ds, R is circular radius, and α is the angle between the direction of ds and x-axis. Since the CA θ on a homogeneous surface is unchangeable and the three-phase contact line shows complete symmetry, the driving force for droplet motion from the surface equals to zero. However, an unbalanced F_s exists in the x-axis direction on some surfaces such as wetting gradient surfaces.[44,45] This driving force is caused by the asymmetric wetting properties and asymmetric water adhesion force at different positions on the sample surface. In this case, the above equation could appropriately be corrected as:

$$dF_s = \gamma R[\cos\theta_A - \cos\theta_R]\cos\alpha d\alpha \quad (2)$$

where θ_A and θ_R are the advancing CA and receding CA, respectively. As shown in Figure 5b, F_s on a non-wetting gradient surface drives small droplets to move from regions with high WCA toward regions with low WCA on the surface, leading to the directional droplet transport behavior.

A droplet self-transport behavior also occurs on a wedge-patterned surface. Under this circumstance, the obvious wettability contrast between the superhydrophobic regions and hydrophilic regions provides a relatively large continuous driving force for the droplet transport. If CAs in the superhydrophobic regions and hydrophilic regions are θ_{sup} and θ_{phi}, respectively, the net surface tension could be expressed as:[46,47]

$$F_{sx} = 2\gamma R[\cos\theta_{phi} - \cos\theta_{sup}][\sin\phi_B - \sin\phi_F] \quad (3)$$

where ϕ_B and ϕ_F are the azimuthal angles at the back boundary and front boundary, respectively, for the hydrophilic and superhydrophobic regions, as shown in Figure 5c. F_{sx} in formula 3 is proportional to the wettability difference in two regions, and a larger difference could generate a greater driving force. Besides, transport behavior of droplets on the wedge-patterned surface is also impacted by the Laplace pressure as another driving force, which is produced by the variations in the fluid surface curvature during this process. When the water

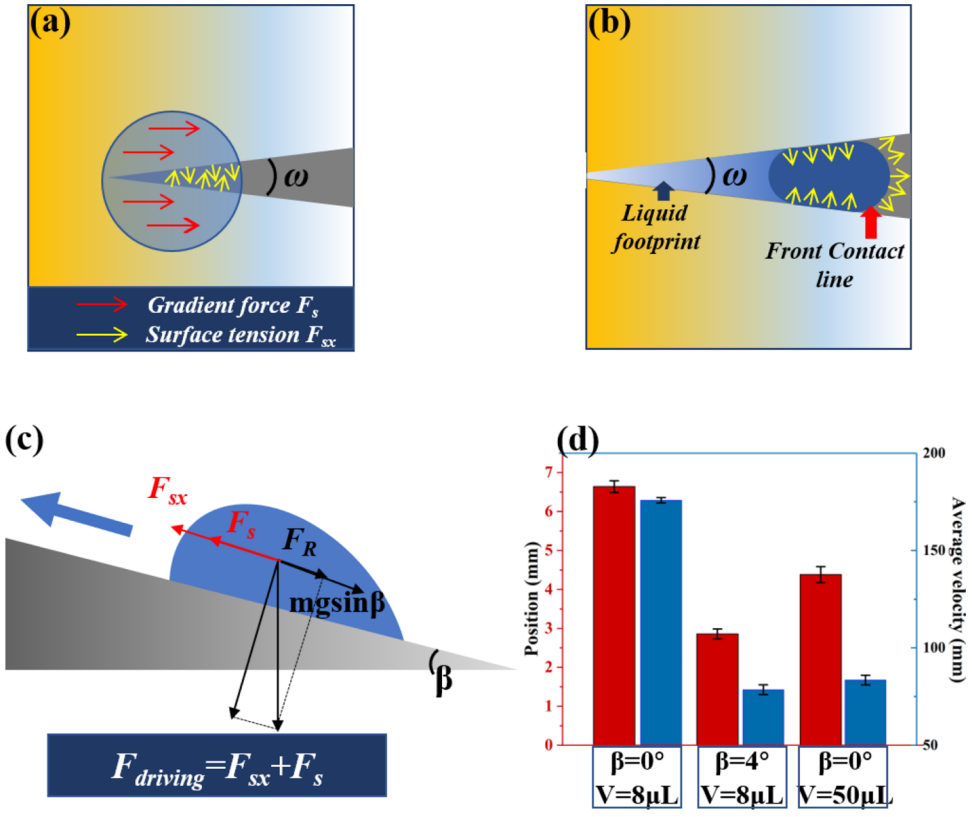

Figure 6. Schematic diagram of droplet force analysis during transportation in different situations. (a) Combined driving force F_d during stage I of droplet transportation. (b) Driving force during stage II of droplet transportation. (c) Diagram of droplet moving upward on an inclined plane. (d) Comparison of droplet transporting distance and average velocity under different inclination angles and droplet volumes on the same surface.

https://doi.org/10.1021/acsomega.3c01536
ACS Omega 2023, 8, 16450−16458

droplet moves toward wider hydrophilic regions, a liquid bulge is formed and the droplet spreads out, causing an unbalanced Laplace pressure, as shown in Figure 5d. The net Laplace pressure as a driving force in the moving direction could be expressed as:[33]

$$\frac{dP}{dx} \sim \frac{d}{dx}\left[\frac{\gamma_{LG}}{r(x)}\right] \sim -\gamma_{LG}\frac{d}{\delta(x)}\left[\frac{2\sin\theta(x)}{\delta(x)}\right]\frac{d\delta(x)}{dx} \sim 2\gamma_{LG}\sin\theta_{avg}\frac{1}{\delta(x)^2} \quad (4)$$

where $\delta(x)$ is the liquid bulge width, $r(x)$ is the curvature of the liquid which satisfies $r(x) = \delta(x)/[2\sin\theta(x)]$, and θ_{avg} is the contact angle over the bulge length. As shown in formula 4, a higher wedge angle leads to a greater Laplace pressure as driving force, so that the droplet has larger transport velocity. However, a larger wedge angle also leads to the increase of contact area between the droplet and hydrophilic regions, causing more resistance and shorter transport distance. In summary, a larger ω on the wedge-patterned surface causes a faster droplet transport velocity and a shorter distance, which is consistent with the experiment results in Figure 3.

The whole transport process could be divided into two stages (stage I and stage II), and droplet transport behaviors depend on different driving force during two stages. Stage I is the initial stage of droplet movement. When the droplet is first placed on the tip end of the wedge-shaped pattern, the circular-shaped three-phase contact line crosses both the hydrophilic region and superhydrophobic region, as shown in Figure 6a. The part of the droplet on the superhydrophobic region is affected by the wetting gradient and moves toward the hydrophilic region rapidly under the impact of chemical gradient force. Meanwhile, the other part of the droplet on the hydrophilic region was influenced by the continuous surface tension and moves toward the wider end of the hydrophilic region. In this situation, the droplet moves with a combining driving force, leading to a larger initial transfer velocity. The combining driving force (F_d) in Figure 6a could be expressed as:

$$F_d = 2\gamma R\int_{\omega/2}^{\pi-\omega/2}[\cos\theta_A - \cos\theta_R]\cos\alpha d\alpha + 2\gamma R[\cos\theta_{phi} - \cos\theta_{sup}][\sin\phi_B - \sin\phi_F] \quad (5)$$

The resistance forces (F_r) could be expressed as:

$$F_r = F_{viscous} + F_{hsyteresis} + F_{friction} + F_{surface\ tension} \quad (6)$$

These four kinds of resistances have been mentioned in the aforementioned work, and the hysteresis force and the viscous force are main resistances during this process.[48] The spontaneous droplet transport occurs under the coaction of driving force and resistance force. After all the droplets moved into the wider hydrophilic region, the transport process enters stage II with a relatively large initial velocity. In stage II, the driving force of the droplets is primarily unbalanced surface tension from the wedge-shaped pattern and Laplace pressure inside the droplet, which is lower than that in stage I, due to the disappearance of driving force from non-wetting gradient. At the same time, water adhesion with the hydrophilic region is clearly larger than that on the superhydrophobic regions; hence, the resistance force also increases at stage II.

Figure 6c presents a schematic diagram of the force analysis of the droplet on an inclined surface. Droplet transport on an inclined surface is subjected to gravity component mgsinβ in the opposite direction. As a result, the moving velocity and distance of the droplet were both reduced compared to that on the horizontal surface. Figure 6d displays the comparison of the droplet transporting distance and average velocity under different inclination angles and droplet volumes on the same surface. A large droplet could still achieve upward transport of water droplets in spite of a greater gravity effect. It could be inferred that a larger droplet possesses more contact areas with the substrate surface, and the width of the droplet contacting the substrate surface exceeds the width of the hydrophilic areas. Therefore, large droplets are driven under a combined driving force of chemical gradient force in the superhydrophobic region and force from the wedge-shaped pattern all over the transport process, and the droplet is maintained in stage I. In summary, a larger droplet is affected by both a greater driving force and higher resistance during the upward transport.

CONCLUSIONS

In summary, non-wetting gradient surfaces with wedge-shaped patterns are fabricated through a combination method of chemical etching, gradient chemical modification, and selective UV irradiation. The superhydrophobic region on the sample surface exhibits a gradient water-repellant characteristic, and the water CA ranged from 160.5° ± 0.2° to 149.2° ± 0.3°. Meanwhile, the water CA on the hydrophilic region gradually drops as UV irradiation time increases and equals 22° ± 0.1° after 1-hour UV irradiation. On this basis, self-transport process of 8 μL droplets is observed on a horizontal sample surface, and a maximum transport displacement of 10.62 mm is achieved on the sample with a wedge angle of 5°, while a maximum average transport velocity of 218.01 mm/s is achieved on the sample surface with a wedge angle of 10°. Besides, self-transport processes of both 8 μL and 50 μL droplets on the inclined surface are evaluated. Finally, theoretical force analysis revealed that driving forces of droplet transport could be divided into three parts: force from non-wetting gradient, unbalanced surface tension from a wedge-shaped pattern, and Laplace pressure inside the droplet. When the three-phase contact line crosses the superhydrophobic and hydrophilic regions, the driving force is the resultant force of the three driving forces. However, when the droplet moves into the hydrophilic region completely, the driving force from non-wetting gradient disappears. Large droplets could not enter the hydrophilic region completely and are subjected to large driving force all over the transport process, increasing the transport distance.

ASSOCIATED CONTENT

Supporting Information

The Supporting Information is available free of charge at https://pubs.acs.org/doi/10.1021/acsomega.3c01536.

Schematic diagram of EDS spectrum for the patterned non-wetting gradient surface after fluorination modification and schematic diagram of the EDS spectrum for the patterned non-wetting gradient surface after UV irradiation for 60 min (PDF)

Spontaneous droplet transport processes in different situations, such as different wedge-angles, inclined

https://doi.org/10.1021/acsomega.3c01536
ACS Omega 2023, 8, 16450−16458

angles, and droplet volumes (AVI) (AVI) (AVI) (AVI) (AVI)

AUTHOR INFORMATION

Corresponding Authors

Yizhou Shen − *Institute of Advanced Materials (IAM), College of Materials Science and Engineering, Nanjing Tech University, Nanjing 211816, P. R. China; College of Materials Science and Technology, Nanjing University of Aeronautics and Astronautics, Nanjing 211100, P. R. China;* orcid.org/0000-0001-8777-5383; Phone: +86 25 52112911; Email: shenyizhou@nuaa.edu.cn

Yaru Ni − *Institute of Advanced Materials (IAM), College of Materials Science and Engineering, Nanjing Tech University, Nanjing 211816, P. R. China*; Phone: +86 25 83587220; Email: nyr@njtech.edu.cn

Authors

Weilan Liu − *Institute of Advanced Materials (IAM), College of Materials Science and Engineering, Nanjing Tech University, Nanjing 211816, P. R. China*

Yang Lu − *Institute of Advanced Materials (IAM), College of Materials Science and Engineering, Nanjing Tech University, Nanjing 211816, P. R. China; College of Materials Science and Technology, Nanjing University of Aeronautics and Astronautics, Nanjing 211100, P. R. China*

Haifeng Chen − *Department of Materials Chemistry, Qiuzhen School, Huzhou University, Huzhou 313000, P. R. China*

Yangjiangshan Xu − *College of Materials Science and Technology, Nanjing University of Aeronautics and Astronautics, Nanjing 211100, P. R. China*

Complete contact information is available at: https://pubs.acs.org/10.1021/acsomega.3c01536

Notes

The authors declare no competing financial interest.

ACKNOWLEDGMENTS

The authors acknowledge the financial support from the National Natural Science Foundation of China (No. 52075246 and U1937206), the Natural Science Foundation of Jiangsu Province (No. BK20211568), the Open Fund of Key Laboratory of Icing and Anti/De-icing (IADL20200107 and IADL20200407), the Basic Research Project of Suzhou (SJC2022032), the Shenyang Key laboratory of Aircraft Icing and Ice Protection (XFX20220301), the project fund by the Priority Academic Program Development of Jiangsu Higher Education Institutions, and project fund by 2022 large instruments and equipment test fee of the Nanjing University of Aeronautics and Astronautics.

REFERENCES

(1) Tani, M.; Kawano, R.; Kamiya, K.; Okumura, K. Towards Combinatorial Mixing Devices Without Any Pumps by Open-capillary Channels: Fundamentals and Applications. *Sci. Rep.* **2015**, *5*, 10263.

(2) Zhao, Y.; Wang, H.; Zhou, H.; Lin, T. Directional Fluid Transport in Thin Porous Materials and its Functional Applications. *Small* **2016**, *13*, No. 1601070.

(3) Si, Y.; Yu, C.; Dong, Z.; Jiang, L. Wetting and Spreading: Fundamental Theories to Cutting-edge Applications. *Curr. Opin. Colloid Interface Sci.* **2017**, *36*, 10−19.

(4) Tian, Y.; Zhu, P.; Tang, X.; Zhou, C. M.; Wang, J.; Kong, T.; Xu, M.; Wang, L. Large-scale Water Collection of Bioinspired Cavity-microfibers. *Nat. Commun.* **2017**, *8*, 1080.

(5) Luo, H.; Lu, Y.; Yin, S.; Huang, S.; Song, J.; Chen, F.; Chen, F.; Carmalt, C. J.; Parkin, I. P. Robust Platform for Water Harvesting and Directional Transport. *J. Mater. Chem. A* **2018**, *6*, 5635.

(6) Zheng, Y.; Bai, H.; Huang, Z.; Tian, X.; Nie, F.; Zhao, Y.; Zhai, J.; Jiang, L. Directional Water Collection on Wetted Spider Silk. *Nature* **2010**, *463*, 640−643.

(7) Shi, Z.; Zeng, H.; Yuan, Y.; Shi, N.; Wen, L.; Rong, H.; Zhu, D.; Hu, L.; Ji, L.; Zhao, L.; Zhang, X. Constructing Superhydrophobicity by Self-Assembly of SiO_2@Polydopamine Core-Shell Nanospheres with Robust Oil-Water Separation Efficiency and Anti-Corrosion Performance. *Adv. Funct. Mater.* **2023**, *33*, No. 2213042.

(8) Li, C.; Lei, W.; Yu, C.; Dong, Z.; Jiang, L. Peristome-mimetic Curved Surface for Spontaneous and Directional Separation of Micro Water-in-oil Drops. *Angew. Chem., Int. Ed.* **2017**, *56*, 13623−13628.

(9) Wang, B.; Liang, W.; Guo, Z.; Liu, W. Biomimetic Super-lyophobic and Super-lyophilic Materials Applied for Oil/water Separation: A New Strategy Beyond Nature. *Chem. Soc. Rev.* **2015**, *44*, 336−361.

(10) Sommers, A. D.; Brest, T. J.; Eid, K. F. Topography-Based Surface Tension Gradients to Facilitate Water Droplet Movement on Laser-Etched Copper Substrates. *Langmuir* **2013**, *29*, 12043−12050.

(11) Li, J.; Qin, Q.; Shah, A.; Ras, R.; Tian, X.; Jokinen, V. Oil Droplet Self-transportation on Oleophobic Surfaces. *Sci. Adv.* **2016**, *2*, No. e1600148.

(12) Bliznyuk, O.; Seddon, J. R. T.; Veligura, V.; Kooij, E. S.; Zandvliet, H. J. W.; Poelsema, B. Directional Liquid Spreading over Chemically Defined Radial Gradient Wettability. *ACS. Appl. Mater. Interfaces* **2012**, *4*, 4141−4148.

(13) Sun, C.; Zhao, X. W.; Han, Y. H.; Gu, Z. Z. Control of Water Droplet Motion by Alteration of Roughness Gradient on Silicon Wafer by Laser Surface Treatment. *Thin Solid Films* **2008**, *516*, 4059−4063.

(14) Chaudhury, M. K.; Whitesides, G. M. How to Make Water Run Uphill. *Science* **1992**, *256*, 1539−1541.

(15) Leng, X.; Sun, L.; Long, Y.; Lu, Y. Bioinspired superwetting materials for water manipulation. *Droplet* **2022**, *1*, 139−169.

(16) Yang, X.; Qi, B.; Lu, Y.; Zhang, W.; Wang, X. Bionic surface diode for droplet steering. *Droplet* **2023**, *2*, No. e46.

(17) Yang, X.; Zhuang, K.; Lu, Y.; Wang, X. Creation of topological ultraslippery surfaces for droplet motion control. *ACS Nano* **2020**, *15*, 2589−2599.

(18) Wu, H.; Zhu, K.; Cao, B.; Zhang, Z.; Wu, B.; Liang, L.; Chai, G.; Liu, A. Smart Design of Wettability-patterned Gradients on Substrate-independent Coated Surfaces to Control Unidirectional Spreading of Droplets. *Soft Matter* **2017**, *13*, 2995.

(19) Sun, J.; Chen, C.; Song, J.; Liu, J.; Yang, X.; Liu, J.; Liu, X.; Lu, Y. A Universal Method to Create Surface Patterns with Extreme Wettability on Metal Substrates. *J. Colloid Interface Sci.* **2018**, *535*, 100−110.

(20) Zhang, S.; Huang, J.; Chen, Z.; Yang, S.; Lai, Y. Liquid Mobility on Superwettable Surfaces for Applications in Energy and The Environment. *J. Mater. Chem. A* **2018**, *7*, 38.

(21) Alheshibri, M. H.; Rogers, N. G.; Sommers, A. D.; Eid, K. F. Spontaneous Movement of Water Droplets on Patterned Cu and Al Surfaces with Wedge-shaped Gradients. *Appl. Phys. Lett.* **2013**, *102*, 146−151.

(22) Wang, Z.; Owais, A.; Neto, C.; Pereira, J. M.; Gan, Y. Enhancing Spontaneous Droplet Motion on Structured Surfaces with Tailored Wedge Design. *Adv. Mater. Interfaces* **2020**, *8*, No. 2000520.

(23) Khoo, H. S.; Tseng, F. G. Spontaneous High-speed Transport of Subnanoliter Water Droplet on Gradient Nanotextured Surfaces. *Appl. Phys. Lett.* **2009**, *95*, No. 063108.

(24) Zheng, Y.; Cheng, J.; Zhou, C.; Xing, H.; Wen, X.; Pi, P.; Xu, S. Droplet Motion on a Shape Gradient Surface. *Langmuir* **2017**, *33*, 4172−4177.

(25) Yin, X.; Wang, D.; Liu, Y.; Yu, B.; Zhou, F. Controlling Liquid Movement on a Surface with a Macro-gradient Structure and Wetting Behavior. *J. Mater. Chem. A* **2014**, *2*, 5620−5624.
(26) Huang, D. J.; Leu, T. S. Fabrication of a Wettability-Gradient Surface on Copper by Screen-printing Techniques. *J. Micromech. Microeng.* **2015**, *25*, No. 085007.
(27) Feng, S.; Wang, S.; Gao, L.; Li, G.; Hou, Y.; Zheng, Y. Controlled Directional Water Droplet Spreading on A High-adhesion Surface. *Angew. Chem., Int. Ed.* **2014**, *53*, 6163−6167.
(28) Wang, J.; Zheng, Z.; Li, H.; Huck, W. T.; Sirringhaus, H. Dewetting of Conducting Polymer Inkjet Droplets on Patterned Surfaces. *Nat. Mater.* **2004**, *3*, 171−176.
(29) Ju, J.; Bai, H.; Zheng, Y.; Zhao, T.; Fang, R.; Jiang, L. A Multi-structural and Multi-functional Integrated Fog Collection System in Cactus. *Nat. Commun.* **2012**, *3*, 1247.
(30) Shen, Y.; Liu, S.; Zhu, C.; Tao, J.; Wang, G. Facile Fabrication of Hierarchical Structured Superhydrophobic Surface and Its Ultra Dynamic Water Repellency. *Chem. Eng. J.* **2017**, *313*, 47−55.
(31) Jin, M.; Shen, Y.; Luo, X.; Tao, J.; Xie, Y.; Chen, H.; Wu, Y. A Combination Structure of Microblock and Nanohair Fabricated by Chemical Etching for Excellent Water Repellency and Icephobicity. *Appl. Surf. Sci.* **2018**, *455*, 883−890.
(32) Ghosh, A.; Ganguly, R.; Schutzius, T. M.; Megaridis, C. M. Wettability Patterning for High-rate, Pumpless Fluid Transport on Open, Non-planar Microfluidic Platforms. *Lab Chip* **2014**, *14*, 1538.
(33) Tan, X.; Zhu, Y.; Shi, T.; Tang, Z.; Liao, G. Patterned Gradient Surface for Spontaneous Droplet Transportation and Water Collection: Simulation and Experiment. *J. Micromech. Microeng.* **2016**, *26*, No. 115009.
(34) Guan, J.; Ruiz-Gutierrez, E.; Xu, B.; Wood, D.; McHale, G.; Ledesma-Aguilar, R.; Wells, G. G. Drop Transport and Positioning on Lubricant-impregnated Surfaces. *Soft Matter* **2017**, *13*, 3404.
(35) Zhang, J.; Han, Y. Shape-gradient Composite Surfaces: Water Droplets Move Uphill. *Langmuir* **2007**, *23*, 6136−6141.
(36) Liu, M.; Yao, Y.; Yang, Y.; Peng, Z.; Chen, S. Directional Transport Behavior of Droplets on Wedge-Shaped Functional Surfaces. *J. Phys. Chem. C* **2019**, *123*, 12736−12743.
(37) Quere, D. Wetting and Roughness. *Annu. Rev. Mater. Res.* **2008**, *38*, 71−99.
(38) Narhe, R. D.; Beysens, D. A.; Pomeau, Y. Dynamic Drying in the Early-Stage Coalescence of Droplets Sitting on a Plate. *Europhys. Lett.* **2008**, *81*, 46002.
(39) Paulsen, J. D.; Carmigniani, R.; Kannan, A.; Burton, J. C.; Nagel, S. R. Coalescence of Bubbles and Drops in an Outer Fluid. *Nat. Commun.* **2014**, *5*, 3182.
(40) Ristenpart, W. D.; McCalla, P. M.; Roy, R. V.; Stone, H. A. Coalescence of Spreading Droplets on a Wettable Substrate. *Phys. Rev. Lett.* **2006**, *97*, No. 064501.
(41) Majid, A.; Lan, C. J.; Arup, D. K.; Ma, Y. Coalescence of Sessile Microdroplets Subject to a Wettability Gradient on a Solid Surface. *Phys. Rev. E* **2016**, *94*, No. 033112.
(42) Berthier, J.; Dubois, P.; Clementz, P.; Claustre, P.; Peponnet, C.; Fouillet, Y. Actuation Potentials and Capillary Forces in Electrowetting Based Microsysterns. *Sens. Actuators, A* **2007**, *134*, 471−479.
(43) Subramanian, R. S.; Moumen, N.; McLaughlin, J. B. Motion of a Drop on a Solid Surface Due to a Wettability Gradient. *Langmuir* **2005**, *21*, 11844−11849.
(44) Zeng, J.; Korsmeyer, T. Principles of Droplet Electro-hydrodynamics for Lab-on-a-chip. *Lab Chip* **2004**, *4*, 265−277.
(45) Gao, L.; McCarthy, T. J. Wetting 101°. *Langmuir* **2009**, *25*, 14105−14115.
(46) Dimitrakopoulos, P.; Higdon, J. J. L. On the Gravitational Displacement of Three-Dimensional Fluid Droplets from Inclined Solid Surfaces. *J. Fluid Mech.* **1999**, *395*, 181−209.
(47) Annapragada, S. R.; Murthy, J. Y.; Garimella, S. V. Droplet Retention on an Incline. *Int. J. Heat Mass Transfer* **2012**, *55*, 1457−1465.
(48) Lenz, P.; Lipowsky, R. Morphological Transitions of Wetting Layers on Structured Surfaces. *Phys. Rev. Lett.* **1998**, *80*, 1920−1923.

https://doi.org/10.1021/acsomega.3c01536
ACS Omega 2023, 8, 16450−16458